A vectorial model for the nonlinear gradient force exerted on metallic Rayleigh nanoparticles

Zheng Zhu (朱 政)[1,2,3], Yuquan Zhang (张聿全)[2], Changjun Min (闵长俊)[2], Aurèle J. L. Adam[3], H. Paul Urbach[3*], and Xiaocong Yuan (袁小聪)[1,2**]

[1] Research Center for Humanoid Sensing, Research Institute of Intelligent Sensing, Zhejiang Lab, Hangzhou 311100, China

[2] Nanophotonics Research Center, Institute of Microscale Optoelectronics & State Key Laboratory of Radio Frequency Heterogeneous Integration, Shenzhen University, Shenzhen 518060, China

[3] Optics Research Group, ImPhys Department, Faculty of Applied Sciences, Delft University of Technology, Delft 2628 CJ, The Netherlands

*Corresponding author: h.p.urbach@tudelft.nl
**Corresponding author: xcyuan@szu.edu.cn

Optical tweezers have proved to be a powerful tool with a wide range of applications. The gradient force plays a vital role in the stable optical trapping of nano-objects. The scalar method is convenient and effective for analyzing the gradient force in traditional optical trapping. However, when the third-order nonlinear effect of the nano-object is stimulated, the scalar method cannot adequately present the optical response of the metal nanoparticle to the external optical field. Here, we propose a theoretical model to interpret the nonlinear gradient force using the vector method. By combining the optical Kerr effect, the polarizability vector of the metallic nanoparticle is derived. A quantitative analysis is obtained for the gradient force as well as for the optical potential well. The vector method yields better agreement with reported experimental observations. We suggest that this method could lead to a deeper understanding of the physics relevant to nonlinear optical trapping and binding phenomena.

Keywords: gradient forces; nonlinear effect; metallic nanoparticles.
DOI: 10.3788/COL202422.023603

1. Introduction

Optical tweezers can exert piconewton forces on small objects and control their motion in the surrounding medium[1,2]. This technique is widely applied in physics[3,4], biology[5], and chemistry[6]. The observation of nonlinear optical trapping presents an anomalous result where two trapping sites can be observed via stimulating the third-order nonlinear effect of dipolar gold nanoparticles, i.e., the "trap split"[7]. Compared with other optical tweezers[8–10], the adjustable distance between two spaced trapping positions can reach beyond the diffraction limit of the focus field without any other complex optical instruments[11–14]. The tunable gap of the trapped particles and the stable manipulation of multiple nanoparticles thereby provide new opportunities for application in atomic and molecular trapping[15], micro-fluid mechanics[16], and bio-medicine[17] at the sub-diffraction-limit scale. The scattering and absorption forces, resulting from the momentum transfer of scattered and absorbed photons, tend to destabilize the trap[18]. The gradient force depends on the distribution of the optical intensity gradients and the polarizability of the nanoparticle[19], which provides the ability to trap the nanoparticle. Therefore, it is crucial to achieve a comprehensive method for the analysis of the nonlinear gradient force exerted on the nanoparticle.

The dipole approximation theory is commonly used to calculate the gradient force exerted on the Rayleigh particle[20,21]. For the particle with a radius much smaller than the wavelength of the incident light, it can be modeled as a dipole[22]. The scalar polarizability can be used to describe the response of the dipole to the external optical field in the linear regime[23]. However, in the nonlinear regime, it is questionable whether the traditional scalar method can still be used to analyze the gradient force being affected by the nonlinear effect. To address this issue, we broaden the traditional scalar method to a vector method to find out whether the nonlinear effect on the gradient force exerted on the metallic nanoparticle can be reflected more explicitly using the vector method.

In our model, the light source is set as a linearly-polarized femtosecond pulsed laser. The gold nanoparticle with a radius of 30 nm is chosen as the metallic model. Using a high NA objective lens to focus the femtosecond pulsed laser, the optical nonlinearity of the gold nanoparticle is stimulated under a correspondingly high level of excitation[24–26]. The tightly-focused
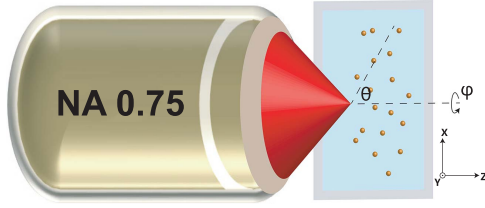
Fig. 1. Configuration of the model. The objective lens with an NA of 0.75 is used.

optical field is decomposed into three-dimensional components using vector diffraction theory[27]. A vectorial polarizability of the dipole is formed by the interplay between the nonlinear optical properties of the dipole and the three components of the tightly focused field. According to the principle of vector superposition, the gradient force along a given direction is expressed based on the interaction between the polarizability vector and the individual components of the optical field. The nonlinear optical potential well can be obtained by integrating the gradient force on the focal plane. In comparison with the gradient force and potential well obtained by using the scalar method, the obvious difference between these two methods is shown at the end. While the model using the scalar method does not give a clear conclusion, the optical potential calculated with the vector method shows that the trapped particles are located along the axis parallel to the direction of linear polarization. The calculation results demonstrate that the vector approach is more consistent with the experimental observations[7]. This new improvement is a step forward in understanding nonlinear optical trapping.

2. Theoretical Model

For a nanoparticle in the Rayleigh regime (radius $\ll \lambda$), the time-averaged forces equation can be written as[21]

$$\langle \mathbf{F} \rangle_{\text{grad}} = \frac{1}{4} \, \text{Re}\{\alpha\} \nabla |\mathbf{E}|^2, \tag{1}$$

with α being the polarizability of the dipole given by

$$\alpha_0 = 4\pi\varepsilon_0 r^3 \frac{n_p^2 - n_h^2}{n_p^2 + 2n_h^2}, \quad \alpha = \frac{\alpha_0}{1 - i\alpha_0 k^3/(6\pi\varepsilon)}, \tag{2}$$

where the complex number n_p is the complex refractive index of the gold nanoparticle, n_h is the refractive index of the host medium, ε is the permittivity of the host medium, r is the particle radius, c is the speed of light in the vacuum, k is the wave number of the incident optical field in the host medium, and $\mathbf{E}$ and $\mathbf{H}$ are the focused electric and magnetic fields.

We show the configuration of the calculation mode in Fig. 1. To excite the nonlinear effect of the particle, it is highly desirable to focus the incident field with a high NA objective lens. In this work, we consider the incident field as an x-polarized, femtosecond laser pulse. Its characteristics are $\tau = 100$ fs, $v = 80$ MHz, x-polarization, and the center wavelength is $\lambda = 840$ nm. The pulsed laser is focused with an objective lens of 0.75 NA inside a glass tube that contains water and gold nanoparticles of 30 nm radius.

2.1. The scalar polarizability of the gold nanoparticle in nonlinear regime

Gold nanoparticles have many nonlinear optical properties that generate great interest in applications such as optical switches[28,29], optical limiting devices[30], and nanoprobes[31]. The optical extinction spectrum of a gold nanoparticle is plotted in Fig. 2(a). The peak of the localized surface plasmon resonance (LSPR) band is at 520 nm, and we choose the near-infrared pulsed laser (central wavelength of 840 nm) as the light source to avoid the SPR effect on the traps.

The linear refractive index of the gold nanoparticles is $n_p = 0.41661 + 5.2347i$[32]. Assuming the average incident power increases from 0 W to 0.5 W, the peak intensity of the focused field I (see Appendix A) is plotted as a function of the incident average power P_{ave} in Fig. 2(b). The intensity-dependent complex refractive index of the gold nanoparticle is described by the Kerr effect equation, $n = n_p + n_2 I$[33,34], where n_2 is the nonlinear refractive index coefficient. Here, the imaginary part of n_2 is set as $-1.16i \times 10^{-16}$ m^2/W, while the real part of n_2 is much smaller than the imaginary part and is set to be zero in our simulations[35,36].
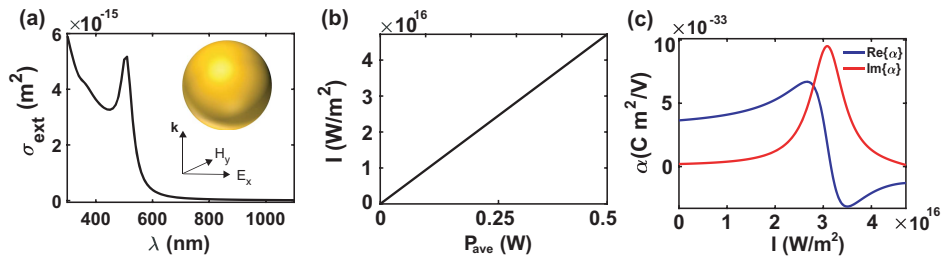

Fig. 2. (a) Extinction spectrum of the spherical gold nanoparticles with a radius of 30 nm. (b) The optical intensity of the focused field is plotted as a function of the average power P_{ave}, increasing from 0 to 0.5 W. (c) The real and imaginary parts of the nonlinear polarizability change with the increasing average power P_{ave}.

By combining the nonlinear refractive index of the gold nanoparticle, we can write the intensity-dependent nonlinear scalar polarizability as

$$\alpha = \frac{4\pi\varepsilon_0 r^3 [(n_p + n_2 I)^2 - n_h^2]/[(n_p + n_2 I)^2 + 2n_h^2]}{1 - \frac{i2\varepsilon_0 k^3 r^3}{3\varepsilon}[(n_p + n_2 I)^2 - n_h^2]/[(n_p + n_2 I)^2 + 2n_h^2]}. \quad (3)$$

The calculation results of the nonlinear scalar polarizability are plotted as a function of the optical intensity in Fig. 2(c). According to Eq. (1), the real part of polarizability $\mathrm{Re}\{\alpha\}$ and the optical intensity gradients determine the magnitude and distribution of the gradient force exerted on the gold nanoparticle. The imaginary part of polarizability $\mathrm{Im}\{\alpha\}$ involves the scattering and absorptive forces, which is not in our scope of discussion.

2.2. The polarizability vector of the gold nanoparticle in the nonlinear regime

The focused electromagnetic field can be calculated using the vectorial diffraction theory[27]. The total electric field **E** is divided into three-dimensional components E_x, E_y, and E_z (see Appendix A). Using Eq. (3), the response of the dipole to each component of the electric field can be calculated individually and form into a polarizability vector. Following the principle of vector superposition, the expression of the polarizability vector can be written as

$$\alpha_i = \frac{4\pi\varepsilon_0 r^3 [(n_p + n_2 I_i)^2 - n_h^2]/[(n_p + n_2 I_i)^2 + 2n_h^2]}{1 - \frac{i2\varepsilon_0 k^3 r^3}{3\varepsilon}[(n_p + n_2 I_i)^2 - n_h^2]/[(n_p + n_2 I_i)^2 + 2n_h^2]}. \quad (4)$$

The polarizability vector is marked as $\boldsymbol{\alpha}_i = \{\alpha_x, \alpha_y, \alpha_z\}$, where i is the Cartesian coordinates ($i = x, y, z$). Combining this with the distribution of the electric field, we can obtain the distribution of the polarizability on the focal plane.

Supposing the average power P_{ave} of the incident laser is 0.5 W, Figs. 3(a)–3(c) show the distribution and magnitude of the three components of the electrical field in the Cartesian coordinate on the focal plane. The x-component of the electric field dominates the total electric field. The real parts of the individual polarizability components $\mathrm{Re}\{\alpha_x\}$, $\mathrm{Re}\{\alpha_y\}$, and $\mathrm{Re}\{\alpha_z\}$ are shown in Figs. 3(d)–3(f), respectively. As can be seen in Fig. 3(d), the sign of $\mathrm{Re}\{\alpha_x\}$ is negative in a certain region due to the nonlinear effect and indicates the reversal of the direction of gradient forces based on the Eq. (1). As shown in Figs. 3(e) and 3(f), the sign inversion of the y- and z-component polarizability does not occur due to the relatively low intensity of the y- and z-components of the electric field. The magnitude of the changes in α_y and α_z is not significant compared to α_x, but their contribution to the calculation of gradient forces in the focal plane should not be ignored.

2.3. The time-averaged gradient force with the vector method

The gradient force on the x–y plane can be considered as the sum of the x- and y- component gradient force. Let $T = 1/v$ be the period of the laser pulses with duration τ; then the time-averaged gradient force $\langle \mathbf{F}\rangle_{\mathrm{grad}}$ in the x- and y- directions can be written as

$$\langle \mathbf{F}_x \rangle_{\mathrm{grad}} = \frac{1}{T}\int_{-\tau/2}^{\tau/2} \frac{1}{4}\sum_i \mathrm{Re}\{\alpha_i\}\frac{\partial |E_i^2|}{\partial_x}\,\mathrm{d}t, \quad (5)$$

$$\langle \mathbf{F}_y \rangle_{\mathrm{grad}} = \frac{1}{T}\int_{-\tau/2}^{\tau/2} \frac{1}{4}\sum_i \mathrm{Re}\{\alpha_i\}\frac{\partial |E_i^2|}{\partial_y}\,\mathrm{d}t, \quad (6)$$

with $i = x, y, z$. Each component of the electric field contributes to the x- and y- component gradient force. After calculating the
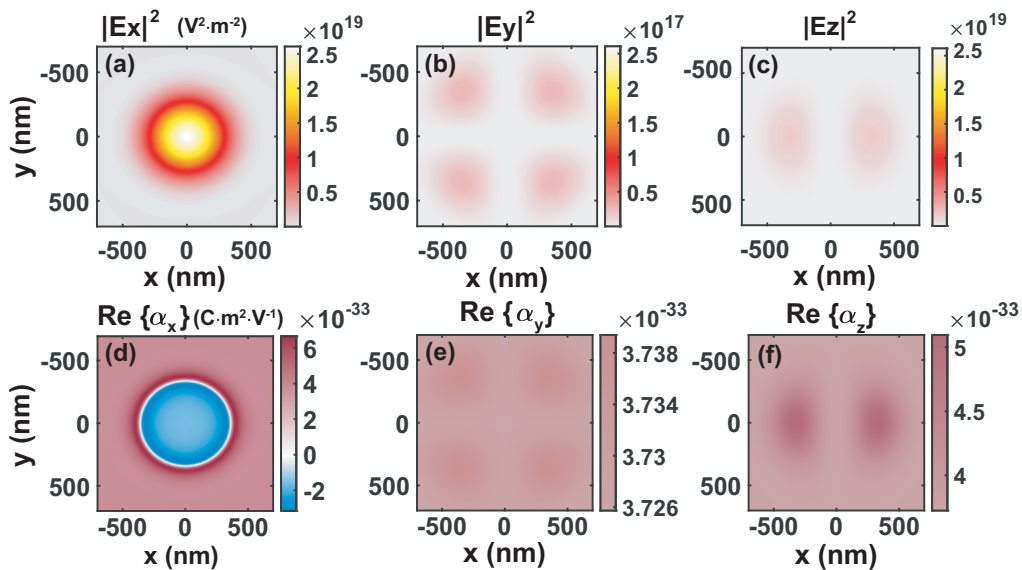

Fig. 3. Distribution of the focused electric field intensity in the focal plane and the corresponding polarizability of the dipolar sphere. (a)–(c) The peak value of the individual field components $|E_x|^2$, $|E_y|^2$, and $|E_z|^2$, respectively. (d)–(f) Real parts of three components of the polarizability $\mathrm{Re}\{\alpha_x\}$, $\mathrm{Re}\{\alpha_y\}$, and $\mathrm{Re}\{\alpha_z\}$.

sum of all the individual forces along a path $\mathbf{r}$, we can calculate the potential well in the focused field as

$$U(\mathbf{r}) = -\int_{\infty}^{r} \langle \mathbf{F}(\mathbf{r}) \rangle d\mathbf{r}. \tag{7}$$

It is worth noting that the gradient force is conservative. The integral path from $\mathbf{r}$ to ∞ is limited to a certain area on the x–y plane, where the net force is a conservative vector field. After carrying out the integration, we obtain the comparison results of the potential well between the use of the scalar and vector methods.

3. Results and Discussion

The x-component gradient force $\langle \mathbf{F}_x \rangle_{\text{grad}}$ generated by the interaction of the x-component of the field intensity gradients $\partial |E_x|^2/\partial x$ and $\text{Re}\{\alpha_x\}$ is shown in Fig. 4(a). The red color indicates that the particle experiences a force along the positive x-axis, while blue indicates a force along the negative x-axis. The magnitudes of $\langle \mathbf{F}_x \rangle_{\text{grad}}$ resulting from the y- and z-components of the electric field are comparatively small, as shown in Figs. 4(b) and 4(c). Figures 4(d)–4(f) show the results of the y-component of the gradient forces derived from each component of the electric field using Eq. (13), respectively. As can be seen in Figs. 4(a) and 4(d), only under the influence of $\text{Re}\{\alpha_x\}$ is the direction of the $\langle \mathbf{F}_x \rangle_{\text{grad}}$ and the $\langle \mathbf{F}_y \rangle_{\text{grad}}$ reversed in the center area of the focal plane.

To further understand the difference between the two methods, we compare the total gradient forces calculated by the scalar and vector methods. The gradient force obtained by the scalar method is shown in Fig. 5(a). The red color indicates that the particle experiences a force towards the center point, while blue indicates that a force is away from the center of the circle. Figure 5(b) shows the vector results as the sum of forces in Figs. 4(a)–4(f). The distribution and magnitude of the gradient forces obtained by these two methods are different, as shown in Figs. 5(c) and 5(d). The black line computed by the vectorial polarizability has a larger maximum value than those calculated by the scalar polarizability in the x-axis, as shown in Fig. 5(c). Figure 5(d) shows the results of the total gradient forces using the scalar method and the vector method in the y-axis, respectively. The total force with α coincides exactly with the results using α in the y-axis. The difference in the results of the x-component of the forces in Fig. 5(c) can be attributed to the use of the vectorial model. In the scalar method, the scalar polarizability is calculated using the total electric field, which approximates the real part of the polarizability along the dominant electric field component (e.g., the x-component for the x-polarized field). However, the scalar method cannot explicitly calculate the contributions of the other components (e.g., y and z) of the electric field and their corresponding polarizabilities ($\text{Re}\{\alpha_y\}$ and $\text{Re}\{\alpha_z\}$). In contrast to the scalar method, the vectorial model calculates the interaction between $\text{Re}\{\alpha_y\}$ and $|E_y|^2$ on the x-axis as well as the interaction between $\text{Re}\{\alpha_z\}$ and $|E_z|^2$ on the x-axis individually. Although the x-component of the electric field dominates the total electric field, the y- and z-components of the electric field also contribute to the force along the x-axis.

To find the position of the trapped particle, we can calculate the corresponding optical potential at the focal plane. The nonlinear optical potential well can be obtained by integrating the total force in Figs. 5(a) and 5(b) on the focal plane.
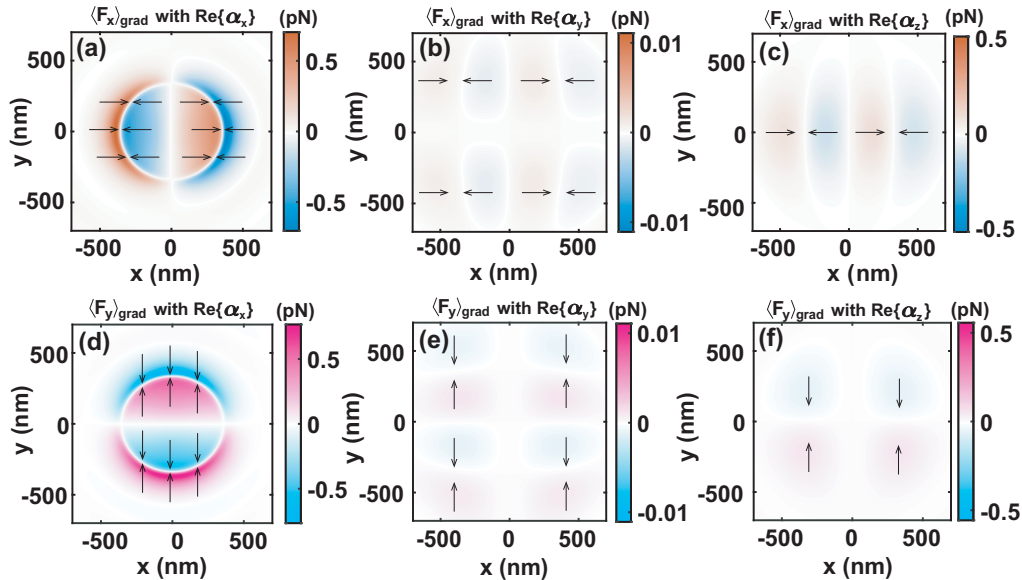

Fig. 4. Nonlinear gradient forces in the focal plane. (a)–(c) The plot of x-component of gradient forces derived from $\text{Re}\{\alpha_x\}$, $\text{Re}\{\alpha_y\}$, and $\text{Re}\{\alpha_z\}$, respectively. Red indicates that the direction of the gradients is along the x-axis, and the force value is positive. Blue denotes the negative force is in the opposite direction of the x-axis. (d)–(f) The plot of y-component of the gradient forces calculated with the vector method. The positive value means the direction of the force is pointing to the y-axis and vice versa for the negative force.
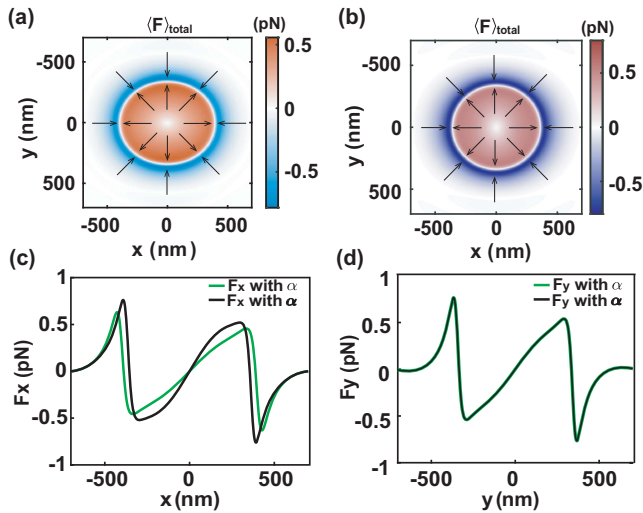
Fig. 5. Total gradient forces obtained by the scalar and vectorial methods. (a) The total gradient forces calculated with the scalar method. (b) The total gradient forces calculated with polarizability vector. (c) Plots of gradient forces along the x-axis for the comparison of two methods. The green line means the gradient force is calculated by the scalar method and the black line for the calculation results based on the vectorial method. (d) The y-component of the gradient forces calculated with scalar polarizability.

Figure 6(a) shows the optical potential well by calculating the polarizability vector. Here, positive and negative values of the potential well indicate that the nanoparticle experiences a repulsive and attractive potential in this plane, respectively. The

coordinate of the minimum potential represents the position of the stable optical trapping. Figures 6(b) and 6(c) show that the minimum potential is located at two points along the x-axis, indicating the presence of two equilibrium positions for the optical trapping. To illustrate the difference between the scalar method and the vector method, potential wells calculated by using the scalar method are plotted in the second rows. The two different methods can both achieve the "trap split" of the optical potential well, as shown in Figs. 6(a) and 6(d). However, parallel projections of the optical potential well reveal the difference between them. The potential well deduced from the scalar method has a "ring-like" depth in the lower part, which means the particle will be trapped in a ring shape, as shown in Figs. 6(e) and 6(f). This result is consistent with the prediction of the vectorial model as shown in Fig. 6(a) and is comparable with the experimental observations reported in Ref. [7] (see Supplementary Material). Therefore, it can be concluded that the scalar method is not able to accurately describe the dipole's response to the tightly focused optical field in nonlinear optical trapping, while the vectorial method provides a more precise description.

It should be noted that, within the linear regime, the optical properties of the nanoparticle remain almost the same, and there is no distinct difference between the scalar method and the vectorial method. In the nonlinear regime, when the peak intensity of each individual component of the electric field is sufficiently high, the third-order nonlinear optical effect can be stimulated, leading to changes in the polarizability of the nanoparticle. In the case of a tightly focused field, the nonlinear optical response
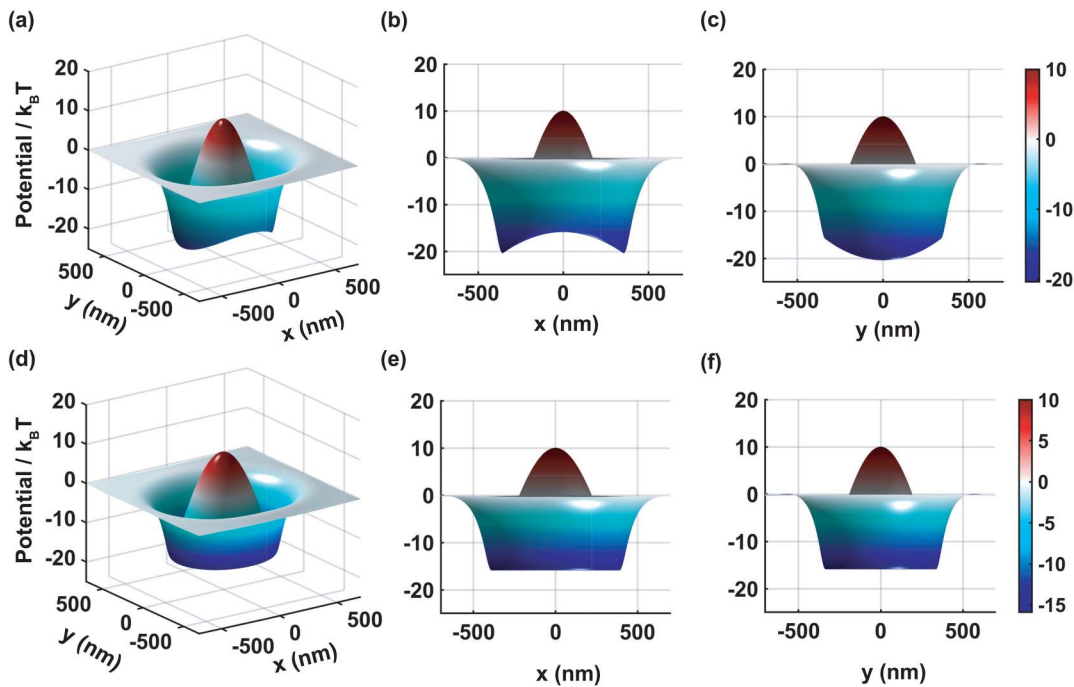

Fig. 6. Nonlinear optical potential well on the focal plane. (a) The nonlinear optical potential well on the focal plane with the vectorial method. (b) The parallel projection of the potential well to the direction of the y-axis. (c) The parallel projection of the potential well to the direction of the x-axis. (d) The potential well with the scalar method. (e) and (f) Parallel projections to the y-axis and x-axis, respectively.

to each individual component of the electric field is different. Therefore, it is necessary to analyze the gradient forces using the vector method to accurately describe the nonlinear optical trapping.

4. Conclusion

In summary, we present an improved vectorial model for the quantitative analysis of nonlinear gradient forces using the polarizability vector of the dipole. The nonlinear polarizability as a function of the optical intensity is obtained after taking the Kerr effect into account. The nonlinear response of a dipolar gold nanoparticle to the tightly focused field is described using the vector diffraction theory, resulting in a polarizability vector. Following the vector approach, we give the individual gradient forces generated by each component of the electric fields on the focal plane. By integrating the total gradient force in the focal plane, the nonlinear potential well is achieved and compared with the experimental results. The study demonstrates that the scalar method is insufficient for analyzing nonlinear optical trapping and that the vectorial model significantly improves the understanding of the phenomena. This approach extends the traditional method from a scalar to a vector model and it has the potential to enhance the development of nonlinear optical tweezers and their related applications.

Appendix A

In addition to the polarizability of the particle, the electromagnetic field also plays an essential role in determining the optical force. To excite the nonlinear effect of the particle, it is highly desirable to focus the incident field with a high NA objective lens. In this work, we consider the incident field as an x-polarized, femtosecond laser pulse. For a femtosecond laser pulse, the peak power of a pulse is estimated from the pulse duration τ and pulse energy E_{pulse},

$$P_{\text{peak}} \approx \gamma \frac{E_{\text{pulse}}}{\tau} = \gamma \frac{P_{\text{ave}}}{\nu \tau}, \qquad (A1)$$

where γ is the factor depending on the temporal shape of the pulse, and ν is the repetition frequency of the pulsed laser. For the Gaussian shape pulse and soliton pulse, the factor is 0.94 and 0.88, respectively[37]. In this paper, we assign to the incident pulse in our analytical model a rectangular temporal envelope and $\gamma = 1$. In this scenario, the strength of the pulse will remain steady over the pulse duration. The peak intensity of the incident beam can be expressed as $I = 2P_{\text{peak}}/\pi r^2$ where the radius of the focal spot $r = 0.82\lambda/\text{NA}$[38]. The peak value of the modulus square of the total electric field $|\mathbf{E}|^2 = 2I_{\text{peak}}/(\varepsilon_0 c n_h)$, where ε_0 is the permittivity of vacuum. The individual component of the electric field can be described using the vectorial diffraction theory. At the excitation wavelength $\lambda = 840$ nm, the wave number in the host medium (water) is k ($k = 2\pi n_h/\lambda$), n_h being the refractive index of host medium.

The maximum focal angle θ_{max} is determined by the NA of the lens and the host medium as $\theta_{\text{max}} = \arcsin(\text{NA}/n_h)$. We use cylindrical coordinates in the focal region given by ρ ($\rho = \sqrt{x^2 + y^2}$), ϕ, and z, where ϕ is the azimuthal angle and z is the coordinate along the optical axis with $z = 0$ corresponding to the focal plane[27],

$$\begin{bmatrix} E_x \\ E_y \\ E_z \end{bmatrix} = E_{00} \begin{bmatrix} I_{00} + I_{02}\cos(2\varphi) \\ I_{02}\sin(2\varphi) \\ -2iI_{01}\cos\varphi \end{bmatrix}, \qquad (A2)$$

$$\begin{bmatrix} H_x \\ H_y \\ H_z \end{bmatrix} = \frac{E_{00}}{Z_{\mu\varepsilon}} \begin{bmatrix} I_{02}\sin(2\varphi) \\ I_{00} - I_{02}\cos(2\varphi) \\ -2iI_{01}\sin\varphi \end{bmatrix}, \qquad (A3)$$

with

$$I_{00} = \int_0^{\theta_{\text{max}}} l(\theta)\sin\theta(1 + \cos\theta)J_0(k\rho\sin\theta)\exp(ikz\cos\theta)d\theta, \qquad (A4)$$

$$I_{01} = \int_0^{\theta_{\text{max}}} l(\theta)\sin^2\theta J_1(k\rho\sin\theta)\exp(ikz\cos\theta)d\theta, \qquad (A5)$$

$$I_{02} = \int_0^{\theta_{\text{max}}} l(\theta)\sin\theta(1 - \cos\theta)J_2(k\rho\sin\theta)\exp(ikz\cos\theta)d\theta, \qquad (A6)$$

where E_{00} is the amplitude of the electric field of the incident light, $Z_{\mu\varepsilon}$ denotes the wave impedance, $J_m(x)$ is the mth order Bessel function of the first kind, and $l(\theta)$ represents the apodization function of the incident field being expressed as

$$l(\theta) = E_{00}\exp[-\sin^2\theta/(f_w\sin\theta_{\text{max}})^2]\sqrt{\cos\theta}, \qquad (A7)$$

where the filling factor f_w is 1 (i.e., the radius ratio of the beam waist to the entrance pupil).

Acknowledgements

References

1. A. Ashkin, J. M. Dziedzic, J. E. Bjorkholm, *et al.*, "Observation of a single-beam gradient force optical trap for dielectric particles," Opt. Lett. **11**, 288 (1986).

2. A. Ashkin, J. Dziedzic, and T. Yamane, "Optical trapping and manipulation of single cells using infrared laser beams," Nature **330**, 769 (1987).

3. Y. Yang, Y. Ren, M. Chen, *et al.*, "Optical trapping with structured light: a review," Adv. Photonics **3**, 034001 (2021).

4. Y. Yu, T.-H. Xiao, Y. Wu, *et al.*, "Roadmap for single-molecule surface-enhanced Raman spectroscopy," Adv. Photonics **2**, 014002 (2020).

5. A. D. Mehta, M. Rief, J. A. Spudich, *et al.*, "Single-molecule biomechanics with optical methods," Science **283**, 1689 (1999).

6. H. Misawa, N. Kitamura, and H. Masuhara, "Laser manipulation and ablation of a single microcapsule in water," Am. Chem. Soc. **113**, 7859 (1991).

7. Y. Jiang, T. Narushima, and H. Okamoto, "Nonlinear optical effects in trapping nanoparticles with femtosecond pulses," Nat. Phys. **6**, 1005 (2010).

8. L. Zhu, Y. Tai, H. Li, *et al.*, "Multidimensional optical tweezers synthetized by rigid-body emulated structured light," Photonics Res. **11**, 1524 (2023).

9. Y. Tan and Y. Gu, "Characteristics of a Gaussian focus embedded within spiral patterns in common-path interferometry with phase apertures," Adv. Photonics **2**, 036008 (2023).

10. L. Zhu, M. Tang, H. Li, *et al.*, "Optical vortex lattice: an exploitation of orbital angular momentum," Nanophotonics **10**, 2487 (2021).

11. Y. Zhang, J. Shen, C. Min, *et al.*, "Nonlinearity-induced multiplexed optical trapping and manipulation with femtosecond vector beams," Nano Lett. **18**, 5538 (2018).

12. L. Huang, Y. Qin, Y. Jin, *et al.*, "Spheroidal trap shell beyond diffraction limit induced by nonlinear effects in femtosecond laser trapping," Nanophotonics **9**, 4315 (2020).

13. Y. Qin, L.-M. Zhou, L. Huang, *et al.*, "Nonlinearity-induced nanoparticle circumgyration at sub-diffraction scale," Nat. Commun. **12**, 3722 (2021).

14. Z. Zhu, Y. Zhang, S. Zhang, *et al.*, "Nonlinear optical trapping effect with reverse saturable absorption," Adv. Photonics **5**, 046006 (2023).

15. S. Chu, J. E. Bjorkholm, A. Ashkin, *et al.*, "Experimental observation of optically trapped atoms," Phys. Rev. Lett. **57**, 314 (1986).

16. R. W. Applegate, J. Squier, T. Vestad, *et al.*, "Optical trapping, manipulation, and sorting of cells and colloids in microfluidic systems with diode laser bars," Opt. Express **12**, 4390 (2004).

17. S. C. Grover, R. C. Gauthier, and A. G. Skirtach, "Analysis of the behaviour of erythrocytes in an optical trapping system," Opt. Express **7**, 533 (2000).

18. V. Wong and M. A. Ratner, "Gradient and nongradient contributions to plasmon-enhanced optical forces on silver nanoparticles," Phys. Rev. B. **73**, 075416 (2006).

19. P. C. Chaumet and M. Nieto-Vesperinas, "Time-averaged total force on a dipolar sphere in an electromagnetic field," Opt. Lett. **25**, 1065 (2000).

20. J. R. Arias-González and M. Nieto-Vesperinas, "Optical forces on small particles: attractive and repulsive nature and plasmon-resonance conditions," J. Opt. Soc. Am. A **20**, 1201 (2003).

21. S. Albaladejo, M. I. Marqués, M. Laroche, *et al.*, "Scattering forces from the curl of the spin angular momentum of a light field," Phys. Rev. Lett. **102**, 113602 (2009).

22. C. F. Bohren and D. R. Huffman, *Absorption and Scattering of Light by Small Particles* (Cambridge University Press, 1983).

23. U. Kreibig and M. Vollmer, *Optical Properties of Metal Clusters* (Springer, 1975).

24. G. Wang, A. A. Baker-Murray, and W. J. Blau, "Saturable absorption in 2D nanomaterials and related photonic devices," Laser Photonics Rev. **13**, 1800282 (2019).

25. L. De Boni, E. L. Wood, C. Toro, *et al.*, "Optical saturable absorption in gold nanoparticles," Plasmonics **3**, 171 (2008).

26. R. W. Boyd, *Nonlinear Optics, 4th* ed. (Academic Press, 2020).

27. L. Novotny and B. Hecht, *Principles of Nano-Optics*, 2nd ed. (Cambridge University Press, 2012).

28. X. Zhang, B. Sun, J. M. Hodgkiss, *et al.*, "Tunable ultrafast optical switching via waveguided gold nanowires," Adv. Mater. **20**, 4455 (2008).

29. Y. H. Lee, Y. Yan, L. Polavarapu, *et al.*, "Nonlinear optical switching behavior of Au nanocubes and nano-octahedra investigated by femtosecond Z-scan measurements," Appl. Phys. Lett. **95**, 023105 (2009).

30. R. West, Y. Wang, and T. Goodson, "Nonlinear absorption properties in novel gold nanostructured topologies," J. Phys. Chem. B **107**, 3419 (2003).

31. S. A. Maier, P. G. Kik, H. A. Atwater, *et al.*, "Local detection of electromagnetic energy transport below the diffraction limit in metal nanoparticle plasmon waveguides," Nat. Mater. **2**, 229 (2003).

32. H.-J. Hagemann, W. Gudat, and C. Kunz, "Optical constants from the far infrared to the X-ray region: Mg, Al, Cu, Ag, Au, Bi, C, and Al$_2$O$_3$," Nat. Mater. **65**, 742 (1975).

33. R. del Coso and J. Solis, "Relation between nonlinear refractive index and third-order susceptibility in absorbing media," J. Opt. Soc. Am. B **21**, 640 (2004).

34. F. Hache, D. Ricard, C. Flytzanis, *et al.*, "The optical Kerr effect in small metal particles and metal colloids: the case of gold," Appl. Phys. A **47**, 347 (1988).

35. R. W. Boyd, Z. Shi, and I. De Leon, "The third-order nonlinear optical susceptibility of gold," J. Opt. Soc. Am. B **326**, 74 (2014).

36. K. Wang, H. Long, M. Fu, *et al.*, "Size-related third-order optical nonlinearities of Au nanoparticle arrays," Opt. Express **13**, 13874 (2010).

37. R. Paschotta, *Field Guide to Laser Pulse Generation* (SPIE Press, 2008).

38. A. Devi and A. De, "Theoretical investigation on nonlinear optical effects in laser trapping of dielectric nanoparticles with ultrafast pulsed excitation," Opt. Express **24**, 21485 (2016).